Fan *et al. Chem Synth* 2024;4:36
**DOI:** 10.20517/cs.2023.72

**Chemical Synthesis**

**Research Article**

**Open Access**

# Microwave-pulse assisted synthesis of tunable ternary-doped 2D molybdenum carbide for efficient hydrogen evolution

**Miao Fan[#], Jiayue Guo[#], Guangyu Fang[#], Haoran Tian, Yongfei You, Zhenhui Huang, Jingru Huang, Huiyu Jiang, Weilin Xu, Jun Wan[*]**

State Key Laboratory of New Textile Materials and Advanced Processing Technologies, Hubei Key Laboratory of Biomass Fibers and Eco-Dyeing & Finishing, Wuhan Textile University, Wuhan 430200, Hubei, China.
[#]Authors contributed equally.

[*]**Correspondence to:** Prof. Jun Wan, State Key Laboratory of New Textile Materials and Advanced Processing Technologies, Hubei Key Laboratory of Biomass Fibers and Eco-Dyeing & Finishing, Wuhan Textile University, 1 Sunny Avenue, Wuhan 430200, Hubei, China. E-mail: wanj@wtu.edu.cn

**How to cite this article:** Fan M, Guo J, Fang G, Tian H, You Y, Huang Z, Huang J, Jiang H, Xu W, Wan J. Microwave-pulse assisted synthesis of tunable ternary-doped 2D molybdenum carbide for efficient hydrogen evolution. *Chem Synth* 2024;4:36. https://dx.doi.org/10.20517/cs.2023.72

**Received:** 27 Dec 2023 **First Decision:** 8 Apr 2024 **Revised:** 13 Apr 2024 **Accepted:** 21 May 2024 **Published:** 21 Jun 2024

**Academic Editor:** Xiang-Dong Yao **Copy Editor:** Dong-Li Li **Production Editor:** Dong-Li Li

## Abstract

Amidst the urgent demand for carbon-neutral strategies, electrocatalytic hydrogen evolution reaction (HER) has garnered significant attention as an efficient and environmentally friendly energy conversion pathway. Non-precious metal layered transition metal carbides, particularly various modified two-dimensional molybdenum carbides (2D $Mo_2C$), have emerged as promising HER catalysts due to their superior intrinsic catalytic activity. While common non-metal doping strategies have been widely employed to enhance the electronic configuration and bulk/interface activity, the mechanism of HER performance dependence on the doping-induced electronic configuration in 2D $Mo_2C$ remains unclear, especially for more complex binary or ternary doping configurations. To address the issue of uncontrollable doping atom percentages in conventional methods, herein, we propose a strategy for rapidly synthesizing highly tunable non-metal multielement-doped 2D $Mo_2C$ using microwave pulse-assisted synthesis. By designing doping configurations with similar atomic ratios, we delve into the impact mechanisms of various doping configurations on the HER performance of 2D $Mo_2C$, with phosphorus doping potentially exerting the most significant positive influence. Furthermore, leveraging the unique thermodynamic and kinetic advantages of microwaves, this approach efficiently prevents potential side reactions associated with multi-element doping, enabling the rapid and precise synthesis of binary and ternary-doped 2D $Mo_2C$. The synthesized

© The Author(s) 2024. **Open Access** This article is licensed under a Creative Commons Attribution 4.0 International License (https://creativecommons.org/licenses/by/4.0/), which permits unrestricted use, sharing, adaptation, distribution and reproduction in any medium or format, for any purpose, even commercially, as long as you give appropriate credit to the original author(s) and the source, provide a link to the Creative Commons license, and indicate if changes were made.

ternary-doped 2D $Mo_2C$ with the same doping atomic ratios (2D P,N,S-$Mo_2C$) exhibits outstanding HER performance. This method not only offers a novel approach for precisely designing non-metallic atomic doping configurations in 2D TMCs but also provides insights into the theoretical structure-activity mechanism for other carbides with unique structures.

**Keywords:** Microwave, 2D material, tunable, ternary-doped, hydrogen evolution

## INTRODUCTION

Electrocatalytic hydrogen evolution reaction (HER), as an efficient and environmentally friendly energy conversion method, has gradually become one of the practical carbon-neutral strategies[1-3]. The widespread application of traditional high-activity Pt-group metal-based electrocatalysts is severely constrained by their high cost and low reserves[4]. Recently, non-precious metal two-dimensional (2D) layered transition metal carbides (TMCs), known as MXenes ($M_{n+1}X_nT_x$:M = early transition metal; X = C or N; $T_x$ = surface termination), and their derivatives have been considered promising HER catalysts[5,6]. Especially 2D molybdenum carbide (2D $Mo_2C$), with its high-density electronic states on the Fermi level *d* orbitals akin to Pt, can effectively enhance excellent intrinsic catalytic activity, while the 2D structure also exposes abundant active sites and facilitates rapid ion transport[7,8]. In order to effectively advance the practical hydrogen production application of 2D $Mo_2C$, it is necessary to further modify and enhance its intrinsic catalytic activity and cycling performance while delving deeper into elucidating the structure-performance relationship in the context of structural engineering [Figure 1A]. Currently, non-metal doping, such as nitrogen doping (N-)[9,10], sulfur doping (S-)[11,12], phosphorus doping (P-)[13,14], fluorine doping (F-)[15,16], *etc*., as a common, straightforward, and efficient strategy to enhance the electronic configuration and bulk/interface activity of energy materials, is ubiquitously employed in various electrocatalytic applications[17-22]. This is primarily because the changes induced by doping, such as alterations in electronegativity, ionization potential, and electron affinity, significantly influence the electronic density and the interactions between molecular and atomic orbitals, thereby shaping the adsorption/desorption behavior of intermediates on the catalyst surface from both electronic configuration and crystal structure perspectives [Figure 1B and C]. For instance, Lv *et al*. demonstrated that N doping greatly altered the electronic configuration of hydrogen-substituted graphdiyne material, contributing to enhanced oxygen reduction reaction (ORR) performance[23]. Zheng *et al*. successfully introduced P doping to $CoSe_2$ material, leading to a phase transition and improved HER performance[24]. Despite the effective alteration of material electronic configuration and interface properties through these non-metal doping processes, there remains a scarcity of reports on the specific impact mechanisms of non-metal doping on the electron configuration-dependent electrocatalytic performance, which holds true for 2D $Mo_2C$. This challenge is primarily constrained by the difficulty of achieving precise control over the doping process using conventional methods. The slow entropy-change reaction processes, represented by solvothermal and high-temperature annealing approaches, make it challenging to attain transient on-off doping reactions, resulting in a random distribution of atomic content of non-metal elements in the final product. The uncontrollable nature of this electronic configuration scenario will significantly impede the elucidation of the structure-performance relationship mechanisms for HER characteristics in structural engineering.

Unfortunately, compared to other HER electrocatalysts with lower synthesis temperatures, such as oxides, sulfides, and phosphides, TMCs typically undergo high-temperature reactions, making it even more challenging to achieve a delicate balance between one-step realization of 2D structural design and precise control of non-metal doping processes. Presently, mainstream methods such as etching MAX [$M_{n+1}AX_n$ ($n$ = 1, 2 or 3) where "M", "A" and "X" are an early transition metal, an element from groups 13-16 in the periodic table, and carbon and/or nitrogen, respectively][25-27] and chemical vapor deposition (CVD)[28-30],

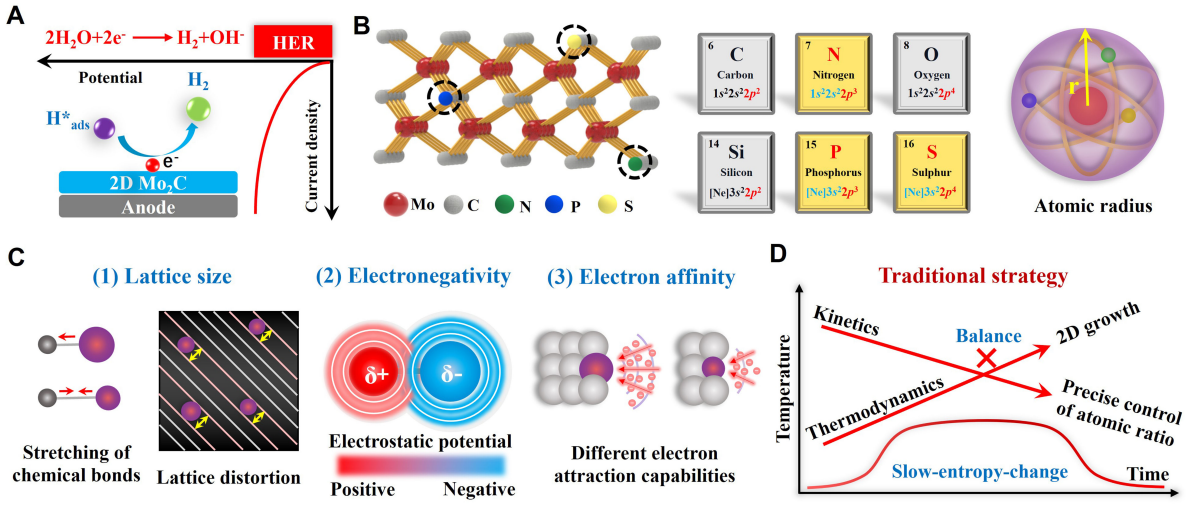


**Figure 1.** Research significance. (A) Mechanism of 2D $Mo_2C$ hydrogen evolution reaction; (B) The reason of doping 2D $Mo_2C$ with P, N and S as an example; (C) Factors affecting electronic structure; (D) The inadequacy of traditional strategy. 2D $Mo_2C$: Two-dimensional molybdenum carbides.

while efficiently producing high-quality 2D $Mo_2C$ and its doped derivatives with excellent HER activity, still have limitations in providing a clear understanding of the impact mechanisms of various non-metal doping on the material's structure and electronic configuration, along with their relationship to electrocatalytic performance [Figure 1D]. Furthermore, unlike single-element doping, binary and ternary doping undergo more complex entropy change processes. In reactions involving potential multiple-doping elements in the precursor, it is highly prone to forming other non-metallic compounds rather than a multi-doped configuration. This is mainly because, in the relatively slow entropy-driven process, chemical reactions tend to favor the thermodynamically stable phase first. For instance, Xie *et al.* utilized urea containing nitrogen and thiourea containing sulfur as precursors, ultimately forming nitrogen-doped sulfides[31]. Similarly, Sun *et al.* utilized tetrahydrate containing nitrogen and ammonium monohydric phosphate containing phosphorus as precursors, generating nitrogen-doped phosphides[32]. This situation is more commonly observed in carbon-nitrogen compounds. These indicate the challenging precision synthesis of doped configurations, significantly impeding the elucidation of the HER performance mechanisms in doped 2D TMCs. Therefore, developing a new strategy to address the seemingly simplest and most direct question - "Under the same doping atomic ratio, which type of non-metallic doping is most advantageous for enhancing the activity of molybdenum carbide" - is crucial for seeking reference answers, holding significant implications for future research and inspiration.

Actually, achieving a balance between the 2D structural design of molybdenum carbide and the precise control of non-metal doping involves a trade-off between the thermodynamics of 2D oriented growth and the kinetics of transient doping processes. Interestingly, over the past decade, advanced non-liquid-phase microwave technology has been able to fully utilize the dipolar, conduction, and magnetic losses to achieve rapid and ultra-high-energy conversion[33,34]. For example, Wan *et al.* demonstrated the rapid synthesis of high-quality graphene using microwave-assisted methods within tens of seconds[35]. Xie *et al.* showed a controllable thermal shock synthesis method based on microwave radiation, enabling the rapid preparation of uniform nanoparticles on graphene[36]. Hu *et al.* used microwave-assisted methods to achieve the 2D structure evolution of TMCs within 3 min[37]. Subsequently, they achieved precise control of metal element doping using microwave discharge[38-40]. These microwave techniques undoubtedly hold significant potential to balance the thermodynamics of 2D oriented growth of $Mo_2C$ with the kinetics of transient doping

processes, successfully enabling the fabrication of various highly tunable non-metal-doped 2D $Mo_2C$ and comprehensively revealing its structure-performance relationship in the context of HER.

Herein, we propose a method for rapidly synthesizing highly tunable non-metal multi-doped 2D $Mo_2C$ using microwave pulse-assisted synthesis. Utilizing the transient on-off characteristics of microwave pulses, controlled doping of molybdenum carbide was achieved by representing the simplest elements, nitrogen, sulfur, and phosphorus, which exhibit distinct extranuclear electron distributions, striking a balance between 2D structural design and precise doping. By designing doping configurations with the same atomic ratio, the impact mechanisms of different types of doping configurations on the HER performance of 2D $Mo_2C$ can be comprehensively elucidated from both electronic configuration and crystal structure aspects, with the positive influence of P doping potentially being the most significant. Moreover, the unique thermodynamic and kinetic advantages of microwaves can effectively prevent side reactions during the doping process. The equiatomic ternary-doped 2D P,N,S-$Mo_2C$ exhibits excellent HER performance (overpotential of 58 mV at a current density of 10 $mA·cm^{-2}$, Tafel value of 48 $mV·dec^{-1}$). The strategy of precisely designing non-metallic atomic doping configurations for 2D TMCs holds the potential to propel the theoretical structure-activity analysis for other carbides with unique structures in electrocatalytic applications.

## EXPERIMENTAL

### Chemicals

All chemicals were commercially acquired and utilized as received without additional purification. The chemical compounds $Na_2MoO_4·2H_2O$ (CAS: 10102-40-6, purity: 99%, analytical reagent grade) and $Na_2S·9H_2O$ (CAS: 1313-84-4, purity: 99.9%, metal-based) were procured from Shanghai Maclin Biochemistry Co., LTD., China. Additionally, Sinopharm Chemical Reagent Co. Ltd. in China provided $C_6H_{12}O_6$ (CAS: 14431-43-7, analytical reagent grade), $H_2C_2O_4$ (CAS: 6153-56-6, analytical reagent grade), $CH_4N_2O$ (CAS: 57-13-6, analytical reagent grade), and $NaH_2PO_4$ (CAS: 7558-80-7, analytical reagent grade).

### Synthesis of 2D P,N,S-$Mo_2C$

Initially, 6 mg $NaH_2PO_4$ (phosphorus source) and 12 mg $Na_2S·9H_2O$ (sulfur source) were added to 1 mL deionized water under the condition that the non-metallic atomic ratio P:N:S = 1:1:1. Then, 60 mg $C_6H_{12}O_6$ (carbon source), 206 mg $Na_2MoO_4·2H_2O$ (molybdenum source), 60 mg $H_2C_2O_4$ (blowing agent) and 1.5 mg $CH_4N_2O$ (nitrogen source) were added, fully mixed, and natural dried for 6 h to obtain a very uniform mixture. The evenly mixed drugs were transferred into a quartz tube with an outer diameter of 16 mm, inner diameter of 12 mm, wall thickness of 2 mm, and length of 60 mm. The tube was placed in a Grant G90F25CN3LN microwave oven for the reaction. First, nitrogen was injected into the reaction chamber for 10 min at a flow rate of 0.8 L/min. Subsequently, the sample was pulse heated three times for 1 min each with an output power of 900 W, under continuous nitrogen flow. After heating, the nitrogen flow was maintained until the apparatus cooled naturally to room temperature. Finally, the samples were taken out, rinsed with distilled water, and desiccated in a vacuum oven at 80 °C for 24 h to obtain 2D P,N,S-$Mo_2C$.

### Synthesis of other doped samples

The same method was used for preparing other doped samples, with the following modifications based on the dopant: A nitrogen-doped 2D $Mo_2C$ (2D N-$Mo_2C$) sample was obtained by adding 1.5 mg $CH_4N_2O$ as a nitrogen source. A phosphorus-doped 2D $Mo_2C$ (2D P-$Mo_2C$) sample was obtained by adding 6 mg of $NaH_2PO_4$ as a phosphorus source. A sulfur-doped 2D $Mo_2C$ (2D S-$Mo_2C$) sample was obtained by adding 12 mg of $Na_2S·9H_2O$ as a sulfur source. A nitrogen and phosphorus-doped 2D $Mo_2C$ (2D P,N-$Mo_2C$) sample was obtained by adding 1.5 mg $CH_4N_2O$ as a nitrogen source and 6 mg $NaH_2PO_4$ as a phosphorus source, respectively. A phosphorus and sulfur-doped 2D $Mo_2C$ (2D P,S-$Mo_2C$) sample was obtained by adding 6 mg

$NaH_2PO_4$ as a phosphorus source and 12 mg $Na_2S·9H_2O$ as a sulfur source, respectively. A nitrogen and sulfur-doped 2D $Mo_2C$ (2D N,S-$Mo_2C$) sample was obtained by adding 1.5 mg $CH_4N_2O$ as a nitrogen source and 12 mg of $Na_2S·9H_2O$ as a sulfur source, respectively. All steps are conducted under specific conditions to ensure the balance between the 2D structure and precise doping.

### Material characterization

The structural composition of the samples was analyzed using X-ray diffraction (XRD) with Cu Kα radiation on an Ultima IV X-ray powder diffractometer and X-ray photoelectron spectroscopy (XPS) using a Thermo Scientific K-Alpha instrument. Their morphologies were examined using high-resolution field emission scanning electron microscopy (FESEM) on a JSM-7800 F instrument (Japan) and transmission electron microscopy (TEM) on a JEM 2100F instrument (Japan). The thickness of 2D P,N,S-$Mo_2C$ was determined by atomic force microscopy (AFM) using a Bruker Dimension Icon instrument (Germany).

### Electrochemical performance

All electrochemical experiments are conducted using rotating disk electrodes (RDEs) of the AFMSRCE model from PINE Instruments in the United States. The electrochemical experiments employed a three-electrode setup with a CHI Electrochemical Station (Model CHI660E, China). As the working electrode, a mirror-polished glassy carbon electrode with a diameter of 0.2 $cm^{-2}$ was utilized, while the reference electrodes included Hg/HgO (1 M KOH) and Ag/AgCl (0.5 M $H_2SO_4$), and the counter electrode was a carbon rod. In a solvent mixture comprising 0.2 mL of deionized water, 0.8 mL of isopropanol, and 20 μL of Nafion (5%, mass fraction), 5 mg of catalyst powder was dispersed. Following that, the mixture underwent ultrasonication in an ice bath for an hour to achieve a homogeneous ink. Afterward, a mirror-polished glassy carbon electrode was drop-cast with 20 μL of the ink, with a catalyst loading of approximately 0.55 $mg·cm^{-2}$. The potential, referenced to a Hg/HgO electrode, was converted to the potential versus the reversible hydrogen electrode (RHE) using E(RHE) = E(Hg/HgO) + E(Hg/HgO *vs.* SHE) + 0.059 pH. The potential, measured against a Ag/AgCl electrode was converted as: E(RHE) = E(Ag/AgCl) + E(Ag/AgCl *vs.* SHE) + 0.059 pH. The electrolyte is placed in a nitrogen atmosphere for at least 30 min before measurement. Using linear scanning voltammetry at a scan rate of 5 $mV·s^{-1}$, polarization curves were recorded at room temperature. The double-layer capacitance ($C_{dl}$) was measured by testing cyclic voltammetry (CV) curves at scan rates ranging from 20 to 200 $mV·s^{-1}$. The electrochemical surface area (ECSA) was calculated based on the $C_{dl}$ of the samples, determined by CV.

The frequency range for electrochemical impedance spectroscopy (EIS) testing was 0.1 to $10^5$ Hz with an amplitude of 10 mV. Long-term durability tests were performed at 10 $mA·cm^{-2}$. The mass activity (MA, $A·g^{-1}$) values of the catalysts were calculated from the catalyst loading ($m$) and measured current density ($i$). MA = $i/m$.

## RESULTS AND DISCUSSION

### Material preparation and characterization

Non-metallic atom P, N, and S doping is a common, simple, and effective strategy to explore the effects of different electronegativity and atomic radius on the band gap, bonding properties, strength, and electron affinity, thus improving the electronic configuration, active sites, and conductivity. The changes in ionic radius, electronegativity, electron affinity, and ionization potential enable adjustments to the electronic structure. Doping with non-metallic heteroatom strategy introduces non-metallic heteroatom, changes electronegativity, electron affinity and ionization potential, and significantly affects the electron structure and local spatial configuration. For example, The P, N and S atoms have larger radii than the C atom, which can promote electron delocalization due to the formation of weaker covalent bonds. Utilizing the transient high-energy and high-temperature advantages of microwave pulses allows for rapid initiation and

termination of the reaction, thereby enabling precise doping of foreign atoms into the host material. The ten-second interpulse pause is consistent with the rapid quenching process, and it is this rapid temperature change that makes the precise doping of non-metallic heteroatoms possible. This approach efficiently mitigates side reactions caused by gradual temperature gradients through rapid heating and cooling performance. This occurs because the quick temperature changes prevent prolonged exposure to intermediate temperature ranges, where unwanted reactions could occur. As a result, the overall reaction proceeds more smoothly and yields the desired products with higher purity. This enhancement in reaction selectivity and efficiency is particularly advantageous in complex chemical processes where precise control over reaction conditions is crucial for the desired outcome. The instantaneous temperature change of microwaves makes it possible to regulate heteroatom doping and 2D structure simultaneously. Because of this property of microwaves, non-metallic elements, which are inherently prone to doping reactions, can almost entirely participate in the reaction at a certain doping level without leakage. Thus, the precise doping of binary/ternary is realized and the 2D structure is constructed in one step.

Considering these factors, the experiment was devised. Figure 2 illustrates the schematic of the microwave-pulse-assisted synthesis of tunable Single/Binary/ternary-doped 2D $Mo_2C$. This setup can operate under various gas conditions, ensuring the requirements of diverse microwave experiments. The detailed configuration of the experimental apparatus is depicted in Supplementary Figure 1. Sodium molybdate tetrahydrate is used as the metal precursor, glucose as the carbon source, oxalic acid as the blowing agent, urea, sodium phosphate and sodium sulfide 9-hydrate as dopants, while ensuring that the atomic ratio about of P:N:S:Mo is 1:1:1:17. It is worth noting that weighing the proportion of metal and non-metal atoms is not strictly consistent with the proportion calculation, because non-metal atoms may partially generate gas outflow during the reaction process, but the microwave pulse method will minimize the extent of this process. The mixture is ground uniformly and placed in a quartz crucible, which is then transferred to a custom microwave reactor surrounded by carbon nanotubes (CNTs). Nitrogen gas is introduced into the system, with its flow meticulously regulated by a flow meter. Real-time monitoring of temperature fluctuations within the reaction zone is achieved using an infrared detector. Throughout the microwave-induced reaction process, the high dielectric constant of CNTs induces dielectric loss, facilitating the rapid and uniform generation of thermal energy within the CNT region. This uniform heating condition is conducive to rapidly introducing non-metal elements and the expedited formation of 2D structures. After the microwave operation, the temperature drops rapidly, resulting in rapid cooling of the reactants, ensuring precise control of the P, N and S atom content. After three microwave pulses, highly tunable non-metallic doped 2D $Mo_2C$ was synthesized in one step striking a balance between kinetics and thermodynamics. In terms of kinetics, the 2D $Mo_2C$ materials doped with single, binary and ternary elements were successfully synthesized using microwave pulses. Regarding thermodynamics, 2D nanosheets were also successfully generated through this method. Utilizing the attributes of real-time controllable microwave pulses facilitates identifying products generated at different stages during the reaction process. Moreover, this capability enables on-site analysis of microwave-induced reactions. Three-dimensional (3D) optical microscopy (OM) was used to characterize the samples with 1, 2, and 3 pulses ($T_1$, $T_2$, and $T_3$, respectively). The results showed three stages of reactants: (1) Polymerization; (2) Bubbling; (3) Burst[37,41-43]. In the initial stage, glucose in the reactants undergoes thermal decomposition and polymerizes into a gel-like polymer during the first pulse. Simultaneously, due to the thermal decomposition of oxalic acid, gas is generated, forming bubbles within the resulting polymer. During the second stage, the temperature inside the reaction chamber remains high for a period, increasing bubbles within the polymer. The release of a large number of bubbles causes the polymer to be blown into a 3D structure. In the third stage, with the extension of reaction time, the gas released by the high-temperature reaction disrupts the 3D bubble structure, generating a large number of 2D nanosheets. The optical images in the figure show that the sample undergoes nearly a seven-fold volume expansion compared to the precursor material after the reaction. Detailed preparation steps are described in the experimental section.

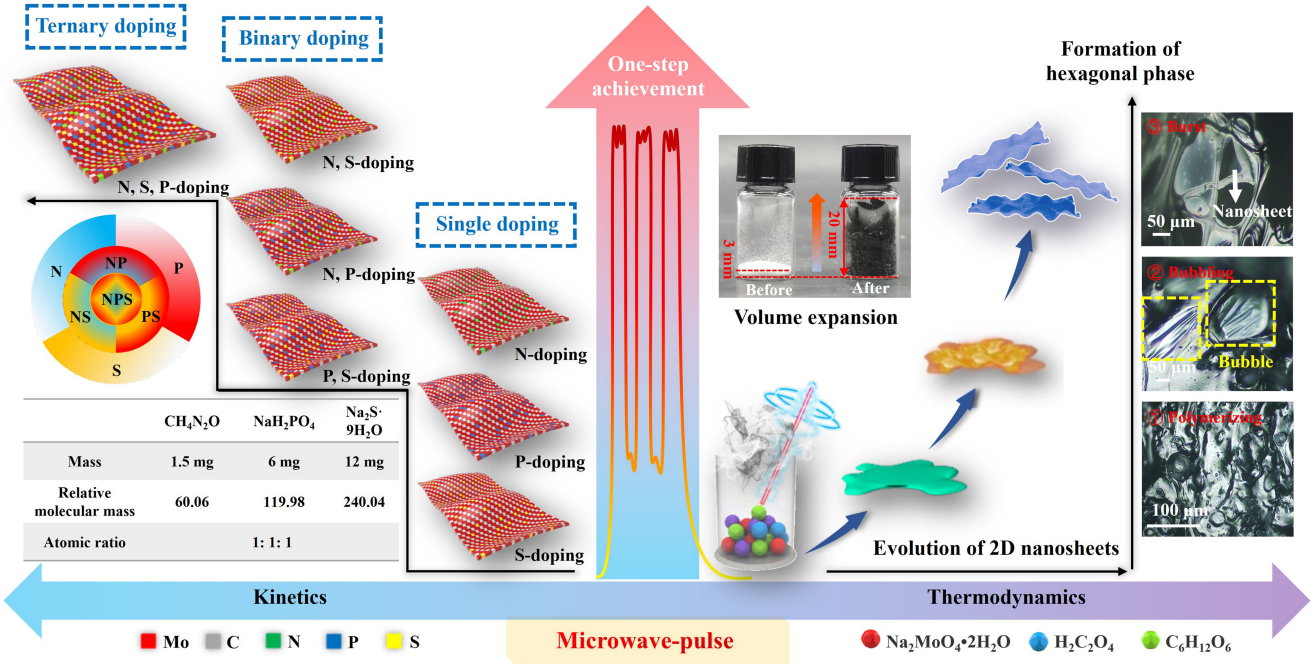


**Figure 2.** Schematic diagram of the influence of microwave pulse strategy on the morphology evolution and doping regulation of 2D $Mo_2C$. 2D $Mo_2C$: Two-dimensional molybdenum carbides.

The temperature change during the reaction was monitored using an infrared detector. As shown in Figure 3A, the reaction zone temperature rapidly reached a relatively stable temperature of 872 °C within 20 s; due to the absorption and reflection of microwaves by CNTs, significant heat conduction is generated. The inserted image displays a physical photograph corresponding to the discharge phenomenon of microwave pulses at 10 s. Due to the excellent capability of CNTs in absorbing microwave radiation, which can be efficiently converted into thermal energy, when exposed to a microwave field, their thermal conductivity aids in the rapid absorption and propagation of microwave energy throughout the entire nanostructure of the nanotubes. Secondly, the inherent structure of CNTs induces pronounced dielectric losses, leading to molecular vibrational excitation and electron friction within the microwave field, thereby culminating in heat generation. This dielectric loss mechanism enables CNTs to effectively absorb microwave energy and convert it into thermal energy. Additionally, the nanoscale dimensions of CNTs endow them with a substantial surface area-to-volume ratio, advantageous for both absorption and dispersion of microwave energy. This nanoscale architecture further facilitates rapid heating and uniform distribution of thermal energy by CNTs within the microwave field, promoting rapid high-temperature carbonization of reactants and rapid doping of non-metallic elements. Once the microwave pulse ceases, the reactants can rapidly decrease to around 271 to 601 °C within 4 s, facilitating rapid cooling of the products, akin to quenching. The experimental device uses pulse heating; each heating cycle lasts 60 s, then pauses for 10 s, and this sequence is repeated three times. In essence, microwave reactions undergo three discernible stages. This is facilitated by the material's exceptional capability to absorb microwaves to quickly raise the desired reaction temperature within 7 s for each microwave pulse. The rapid heating and cooling characteristics reduce the likelihood of side reactions induced by temperature gradients, facilitating precise doping of heteroatoms. The morphology of the samples after the reaction was then characterized. Scanning electron microscopy (SEM) characterization of the catalyst morphology was performed [Figure 3B], revealing that the obtained P,N,S-$Mo_2C$ exhibits a large 2D nanosheet structure with a smooth and flexibly curled surface, with lateral dimensions reaching up to 30 μm. This significantly increases the

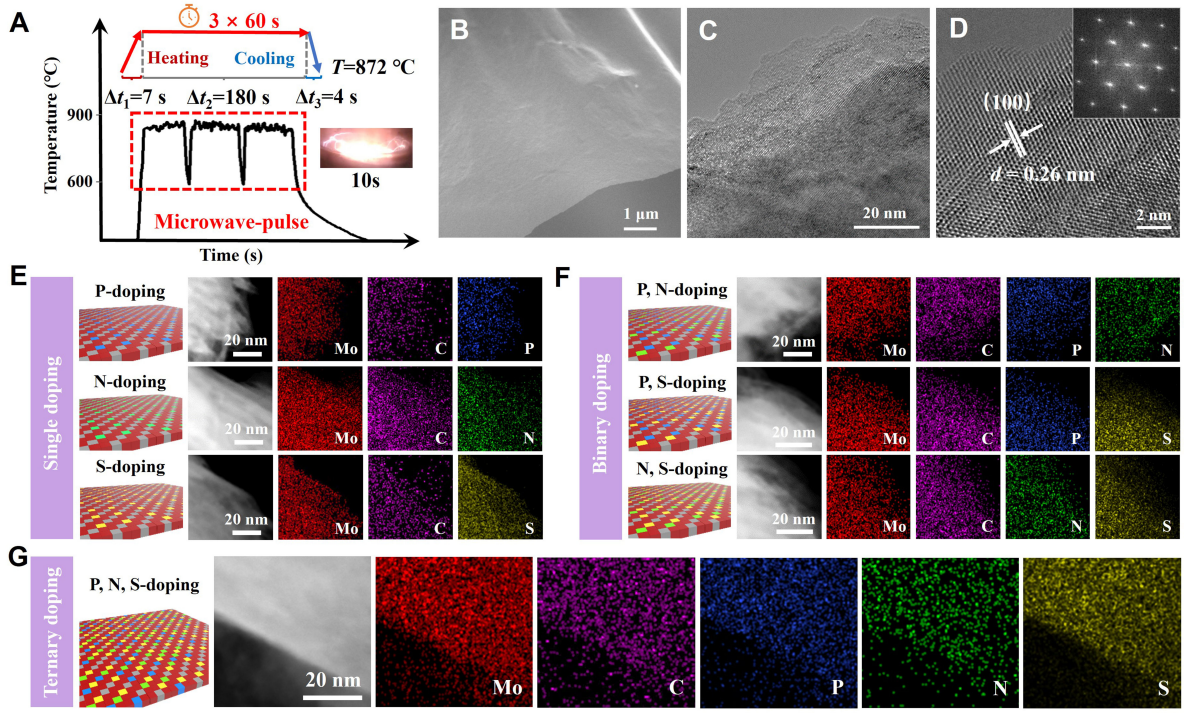


**Figure 3.** Morphology characterization. (A) Real-time temperature changes of samples heated by microwave pulses. The inset image is 10 s microwave discharge diagram; (B) SEM images of 2D P,N,S-$Mo_2C$; (C) TEM images of 2D P,N,S-$Mo_2C$; (D) The HRTEM image of 2D P,N,S-$Mo_2C$ and the insert image is the corresponding SAED pattern; (E) EDS elemental mapping scanning from TEM of single doping 2D $Mo_2C$; (F) EDS elemental mapping scanning from TEM of binary doping 2D $Mo_2C$; (G) EDS elemental mapping scanning from TEM of ternary doping 2D $Mo_2C$. 2D: Two-dimensional; $Mo_2C$: molybdenum carbides; SEM: scanning electron microscopy; TEM: transmission electron microscopy; HRTEM: high-resolution transmission electron microscopy; SAED: selected area electron diffraction; EDS: energy-dispersive X-ray spectroscopy.

electrochemical active sites and surface area, conducive to enhanced electrocatalytic performance. The other six types of single/binary-doped $Mo_2C$ also displayed apparent 2D structures, and the morphology was basically the same as that of 2D P,N,S-$Mo_2C$ [Supplementary Figure 2], indicating that doping did not affect the 2D structure of the sample [Supplementary Figure 3]. Using Atomic Force Microscopy (AFM), the thickness of the P,N,S-$Mo_2C$ nanosheets was measured; analysis revealed a thickness of 2 nm [Supplementary Figure 4]. TEM images in Figure 3C also confirmed the ultra-thin thickness of the P,N,S-$Mo_2C$ nanosheets. The corresponding high-resolution transmission electron microscopy (HRTEM) images [Figure 3D], exhibit clear lattice fringes with a spacing of 0.26 nm, corresponding to the (100) plane of $Mo_2C$, further indicating the successful synthesis of the $Mo_2C$ phase. Additionally, the selected area electron diffraction (SAED) pattern in the upper right corner of the HRTEM image showed that P,N,S-$Mo_2C$ is a single crystalline hexagonal phase. Compared to traditional heating methods, the microwave pulse heating and cooling process ensures rapid carbonization while simultaneously facilitating the doping process, avoiding side reactions during doping and favoring the formation of single-crystal structures. The element mapping and corresponding elemental mappings, along with the Energy Dispersive X-ray Spectroscopy (EDX) spectra of 2D $Mo_2C$ doped with heteroatoms, show a uniform distribution of elements [Figure 3E-G]. This confirms that the microwave-pulse-assisted strategy effectively achieved precise doping of non-metal elements P, N, and S into 2D $Mo_2C$, while also constructing the 2D structure in a single step.

Leveraging the unique attributes of microwave pulse assistance, we can characterize the structural evolution of the samples at different stages of the reaction. The XRD data were refined using General Structure

Analysis System (GSAS) software [Figure 4A]. The parameters of the synthesized catalyst were calculated, and the changes related to atomic doping were revealed. As shown in Supplementary Table 1, the lattice parameters increase from 3.0124 Å, 3.0124 Å, 4.7352 Å to 3.0150 Å, 3.0150 Å and 4.7476 Å, respectively. The lattice size of 2D P,N,S-$Mo_2C$ is larger than pristine $Mo_2C$. This is because the atomic radius of C is different from that of P, N, and S atoms, suggesting that various types of non-metallic heteroatoms have been successfully incorporated into the lattice of $Mo_2C$. As shown in Supplementary Figure 5, the XRD data for samples subjected to one, two, and three microwave pulses clearly demonstrate the structural evolution of 2D P,N,S-$Mo_2C$. After the first pulse, the XRD spectrum between 15° and 30° shows a broad diffraction peak, possibly due to the thermal decomposition of glucose resulting in a large amount of carbon. Following the second pulse, the XRD features are predominantly those of monoclinic $MoO_2$ (PDF: 01-076-1807)[44]. The formation of $Mo_2C$ single crystal phase is observed after the third pulse. The diffraction peaks of the obtained 2D P,N,S-$Mo_2C$ at 34.3, 37.9, 39.3, 52.1, 61.5, 69.5, 72.3, 74.6, and 75.5, when compared with the collection code (023823) from the Inorganic Crystal Structure Database (ICSD), correspond to the hexagonal phase $Mo_2C$ (PDF: 00-035-0787) planes of (100), (002), (101), (102), (110), (103), (200), (112), and (201), respectively[45]. Doping does not cause obvious change of crystal structure, suggesting that the microwave-pulse-assisted synthesis of 2D P,N,S-$Mo_2C$ does not produce any by-products.

Subsequently, XPS was employed to investigate the oxidation states of elements in the non-metal-doped 2D Mo2C samples and the bonding of surface elements in depth. As depicted in Figure 4B, the high-resolution Mo 3*d* spectrum can be resolved into four doublets. The two prominent peaks at 228.6 and 232.0 eV correspond to $Mo^{2+}$ (Mo $3d_{3/2}$ and Mo $3d_{5/2}$), indicating $Mo_2C$ bonds. Concurrently, the presence of $Mo^{3+}$ peaks at 229.0 and 232.8 eV suggests potential P–Mo and N–Mo bonding. The presence of $Mo^{3+}$ indicates that P or N occupies part of the C position in $Mo_2C$, which may optimize its electronic properties and reduce the desorption energy of the Mo–H bond. The valence states of $Mo^{4+}$ (230.4 and 233.8 eV) and $Mo^{6+}$ (233.1 and 236.2 eV) may be associated with the inevitable surface oxidation of Mo exposed to air[46]. In the C 1*s* spectrum, the peak at 284.0 eV, attributed to the Mo–C bond, further confirms the formation of the $Mo_2C$ phase. The peaks at 288.8, 286.6, 285.4, and 284.7 eV correspond to O–C=O, C=O, C–O and C–C bonds, respectively[47,48] [Supplementary Figure 6]. The presence of oxygen groups (O–C=O) is beneficial for enhancing the wettability of the catalyst to the electrolyte[49]. The peaks at 129.4 and 130.4 eV in the P 2*p* spectrum correspond to the P $2p_{3/2}$ and p $2p_{1/2}$, respectively. [Figure 4C]; all these peaks are associated with the P–Mo bonds after doping. The peak at 133.3 eV corresponds to the P–C bond, while the peak at 134.2 eV corresponds to the P-O signal, likely due to oxidation upon exposure to air[46,50]. This provides evidence for successful doping of P heteroatoms into $Mo_2C$. Figure 4D presents the high-resolution spectrum of N 1s. Peaks at 394.7, 398.36, 399.48, and 401.26 eV are ascribed to Mo-N, pyridinic N, pyrrolic N, and graphitic N, respectively[46,51]. The presence of C-N indicates successful incorporation of N atoms into the $Mo_2C$ phase via microwave thermal pulse, with N incorporation potentially influencing the catalytic activity of $Mo_2C$. High-resolution S 2*p* spectrum [Figure 4E] reveals double peaks at 162.2 and 163.3 eV, corresponding to S $2p_{3/2}$ and S $2p_{1/2}$, respectively, indicating successful S doping into $Mo_2C$. Additionally, double peaks at 163.9 and 165.1 eV correspond to S $2p_{3/2}$ and S $2p_{1/2}$ of the C–S–C bond, while oxidized S is observed at 169.0 eV[46,50]. Thus, the XPS results confirm successful co-doping of non-metal atoms P, N, and S into $Mo_2C$, which will further modulate the electronic structure of the electrocatalyst, playing a significant role in the catalytic activity of $Mo_2C$. An important point to note is that the atomic ratios of P, N and S remain the same after statistical analysis of the composition of 2D $Mo_2C$ doped by non-metallic atoms, each accounting for about 3% ± 0.09% of the total composition [Figure 4F]. This is basically consistent with the proportion of atoms weighed before the reaction, indicating little loss of non-metallic atoms under the high-energy impact of microwave pulses. This shows that the microwave pulse method not only successfully achieves the design of 2D structures but also can precisely control the percentage of atoms, a feat difficult to achieve with traditional methods. It is worth noting that the precise regulation of non-metallic atoms by

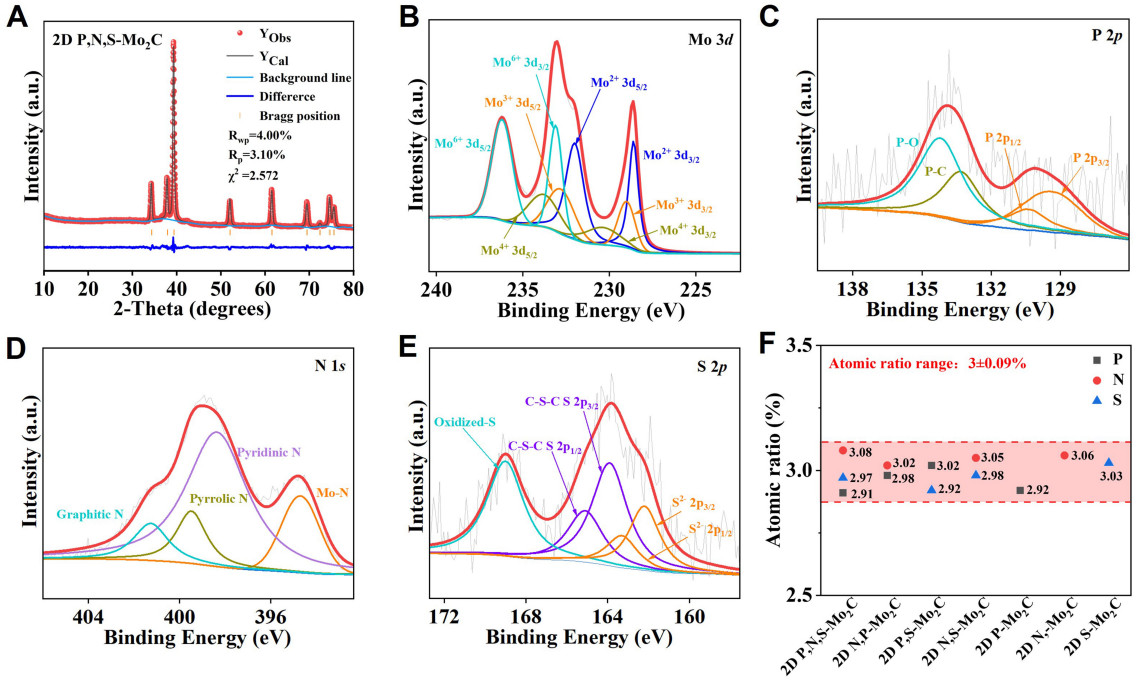


**Figure 4.** Structural characterization. (A) Difference patterns for the Rietveld refinement from the XRD of 2D P,N,S-$Mo_2C$; (B-E) High-resolution XPS spectra of Mo 3*d*, p 2*p*, N 1s and S 2*p* of 2D P,N,S-$Mo_2C$; (F) Summary of the proportion of each heteroatom in 2D doped-$Mo_2C$. XRD: X-ray diffraction; 2D: two-dimensional; $Mo_2C$: molybdenum carbides; XPS: X-ray photoelectron spectroscopy.

microwave pulses is not limited to equal doping; if the ratio of P to S in the initial reactant is changed to 2:1, it is also feasible to achieve a 2:1 ratio of P:S atoms in the final product of the reaction. Meanwhile, due to the small proportion of non-metallic atom doping, the number of non-metallic atoms involved in doping is far less than the number of sites that can be replaced, so the competition between doping atoms in this process can be ignored. Additionally, as demonstrated in Supplementary Figures 7 and 8, the high-resolution spectra for each element in 2D P-$Mo_2C$, 2D N-$Mo_2C$, 2D S-$Mo_2C$, 2D P,N-$Mo_2C$, 2D P,S-$Mo_2C$, and 2D N,S-$Mo_2C$ further substantiate the high applicability of non-metal doping in 2D $Mo_2C$ using the microwave-pulse method.

## Hydrogen evolution performance test

By designing a similar doping atom ratio, the influence of P, N, S doping on electron configuration of non-metallic atoms with different electronegativity and atomic radii can be analyzed. Electrochemical testing can systematically investigate the HER performance mechanism dependent on various electron configurations. In acidic media, HER can be divided into two steps[52]: firstly, the adsorption of $H^+$, known as the Volmer reaction ($H_3O^+ + e^- \rightarrow H^*_{ads} + H_2O$), followed by the desorption step, known as the Heyrovsky reaction ($H^*_{ads} + H_3O^+ + e^- \rightarrow H_2 + H_2O$), or the recombination step, known as the Tafel reaction ($H^*_{ads} + H^*_{ads} \rightarrow H_2$). Therefore, a large amount of electron and ion transfer is involved, and 2D materials can provide an abundant active site for HER reaction and rapid electron and ion transfer speed [Figure 5A].

Figure 5B shows the polarization curves of 2D $Mo_2C$, 2D P-$Mo_2C$, 2D N-$Mo_2C$, 2D S-$Mo_2C$, 2D P,N-$Mo_2C$, 2D P,S-$Mo_2C$, 2D N,S-$Mo_2C$ and 2D P,N,S-$Mo_2C$ s in 0.5 M $H_2SO_4$. To provide a benchmark for comparison, the electrocatalytic activity of a commercial Pt/C catalyst was measured under identical conditions. The HER potential corresponding to a current density of 10 mA·cm$^{-2}$ is plotted in Figure 5C. Notably, At a current density of 10 mA·cm$^{-2}$, the overpotential of 2D P,N,S-Mo2C is 58 mV, which is close

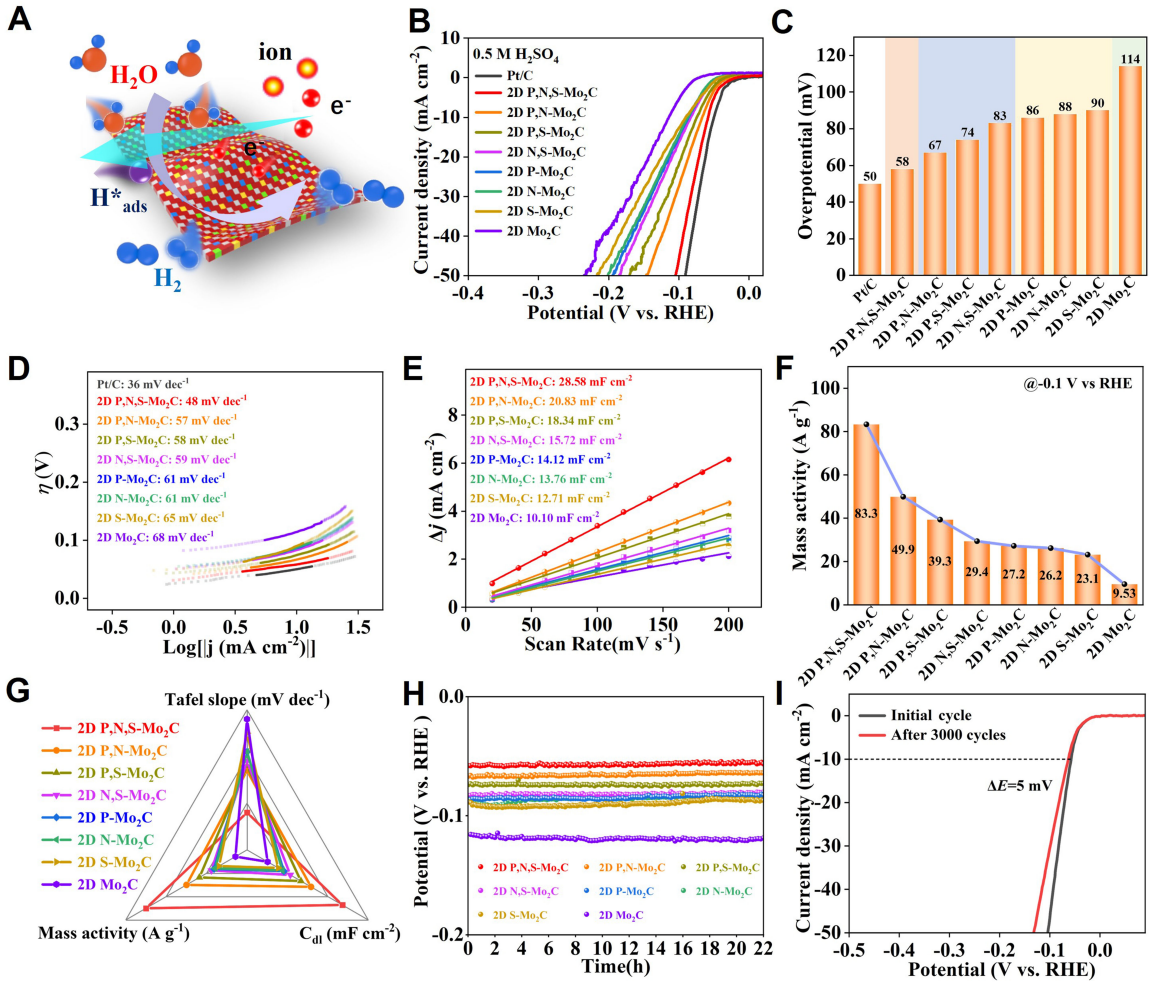


**Figure 5.** Synthesis of doped 2D $Mo_2C$ in 0.5 M $H_2SO_4$ electrocatalytic HER by microwave pulse method. (A) Schematic diagram of HER reaction for rapid electron and ion transport 2D P,N,S-$Mo_2C$ nanosheets; (B) Polarization curve; (C) Overpotentials at 10 mA·cm$^{-2}$; (D) The corresponding Tafel slope; (E) Plotting current density variation against scan rate to fit linear regression allows for the estimation of $C_{dl}$; (F) Mass activity of various spinels calculated at -0.1 V *vs.* RHE; (G) Summary of statistical electrochemical properties; (H) Chronopotentiometry test at the current density of 10 mA·cm$^{-1}$; (I) The accelerated durability tests of 2D P,N,S-$Mo_2C$. 2D: Two-dimensional; $Mo_2C$: molybdenum carbides; HER: hydrogen evolution reaction; RHE: reversible hydrogen electrode.

to that of Pt/C (50 mV) and surpasses 2D P-$Mo_2C$ (86 mV), 2D N-$Mo_2C$ (88 mV), 2D S-$Mo_2C$ (90 mV), 2D P,N-$Mo_2C$ (67 mV), 2D P,S-$Mo_2C$ (74 mV) , 2D N,S-$Mo_2C$ (83 mV) and much better than 2D $Mo_2C$ (114 mV). Due to the doping of non-metallic atoms replacing some carbon atoms and the differences in electronegativity and atomic size between carbon and non-metallic atoms, the intrinsic electronic structure of carbon is altered, creating new active sites and ultimately enhancing catalytic activity[53-55]. These changes break the symmetry of the electric neutrality and/or spin distribution, resulting in charge/spin redistribution that favors the adsorption of HER intermediate species and promotes HER catalytic reactions[55]. At the same time, co-doping with multiple non-metallic dopants not only increases the defect concentration but also generates synergistic effects between different non-metallic dopant atoms[56,57], which can form P–N bonds to regulate the electronic structure with strong synergistic coupling effects, while N and S dopants have synergistic effects as σ-donors and π-inverse-donors, which help improve the adsorption efficiency, weaken the hydroxide bonds, and promote the generation of $H_2$. These effects significantly enhance the

catalytic activity of 2D P,N,S-$Mo_2C$[58-60]. The Tafel slope can be used as an important parameter to judge the kinetic properties of HER. Figure 5D provides the Tafel values corresponding to the polarization curves. The Tafel slope of the 2D P,N,S-$Mo_2C$ sample is 48 mV·dec$^{-1}$, still superior to 2D P-$Mo_2C$ (61 mV·dec$^{-1}$), 2D N-$Mo_2C$ (61 mV·dec$^{-1}$), 2D S-$Mo_2C$ (65 mV·dec$^{-1}$), 2D P,N-$Mo_2C$ (57 mV·dec$^{-1}$), 2D P,S-$Mo_2C$ (58 mV·dec$^{-1}$), and 2D N,S-$Mo_2C$ (59 mV·dec$^{-1}$), and significantly better than 2D $Mo_2C$ (68 mV·dec$^{-1}$). Incorporating appropriate amounts of electron-rich dopants, such as phosphorus, into the $Mo_2C$ lattice mitigates the density of vacant d orbitals, thereby weakening the robust Mo–H bonds within $Mo_2C$, and promoting the $H^*_{ads}$ desorption (Heyrovsky/Tafel) step promotes HER kinetics[61,62]. In order to further understand the underlying mechanism of enhancing HER activity with non-metallic doped $Mo_2C$ catalyst, the electrochemical active area (ECSA) was estimated by testing the $C_{dl}$. The CV curves of samples with eight samples are measured in the voltage range of 0.1~0.2 V (*vs.* RHE) are shown in Supplementary Figure 9. As depicted in Figure 5E, 2D P,N,S-$Mo_2C$ exhibits a $C_{dl}$ of 28.58 mF·cm$^{-2}$, much larger than those of 2D P-$Mo_2C$ (14.12 mF·cm$^{-2}$), 2D N-$Mo_2C$ (13.76 mF·cm$^{-2}$), 2D S-$Mo_2C$ (12.71 mF·cm$^{-2}$), 2D P,N-$Mo_2C$ (20.83 mF·cm$^{-2}$), 2D P,S-$Mo_2C$ (18.34 mF·cm$^{-2}$) , 2D N,S-$Mo_2C$ (15.72 mF·cm$^{-2}$) and 2D $Mo_2C$ (10.10 mF·cm$^{-2}$). This indicates that 2D P,N,S-$Mo_2C$ possesses more catalytically active sites than other catalyst components, which can be ascribed to difference in atomic radius formed by P, N and S non-metallic elements doped with 2D $Mo_2C$, which may lead to lattice distortion or formation of defective structures. These distortions and defects can provide more active sites and alter the surface electronic structure, thereby promoting electrocatalytic reactions[63]. The parameter of MA serves as a crucial metric for characterizing the intrinsic Hydrogen Evolution Reaction (HER) efficiency of catalysts. Figure 5F shows the MA value at -0.1 V *vs.* RHE. Notably, The MA of 2D P,N,S-$Mo_2C$ was 83.3 A·g$^{-1}$, 8.74 times higher than that of 2D $Mo_2C$ (9.53 A·g$^{-1}$). The observed variations in apparent MA among these catalysts indicate that the heightened activity is attributed to the internal electronic structure modulation by non-metallic atoms P, N, and S. As illustrated in Figure 5G, a more intuitive reveals that the 2D P,N,S-$Mo_2C$ exhibits superior performance across various metrics compared to other samples, notably surpassing the 2D $Mo_2C$. This further substantiates the enhanced electrocatalytic properties of the 2D P,N,S-$Mo_2C$. Moreover, the EIS measurement results align with the trends in the polarization curves [Supplementary Figure 10]. Compared with other electrocatalysts, The radius of 2D P,N,S-$Mo_2C$ is the smallest, indicating that 2D P,N,S-$Mo_2C$ has the smallest charge-transfer resistance ($R_{ct}$). The $R_{ct}$ values of 2D P-$Mo_2C$, 2D N-$Mo_2C$, 2D S-$Mo_2C$, 2D P,N-$Mo_2C$, 2D P,S-$Mo_2C$, 2D N,S-$Mo_2C$, 2D $Mo_2C$ and 2D P,N,S-$Mo_2C$ were 37, 41, 43, 19, 20, 28, 47 and 16 Ω, indicating that the addition of P, N and S atoms effectively reduces the electrode resistance, resulting in better conductivity and charge transfer rate of 2D P,N,S-$Mo_2C$, thereby improving the electrochemical HER. This shows that the doping of P, N and S atoms with 2D $Mo_2C$ can effectively reduce the electrode resistance. These results are consistent with the Tafel plots. Additionally, long-term stability is a key parameter for evaluating HER catalysts and their electrocatalytic activity. Figure 5H illustrates the long-term stability of seven samples at a current density of 10 mA·cm$^{-2}$ measured by chronoamperometry. The results show that after 22 h of uninterrupted operation in the alkaline electrolyte, the potential of the sample has almost no change, showing excellent stability. Subsequently, the $C_{dl}$ after the long-term stability test was characterized [Supplementary Figure 11], and it was found that there was no significant change before and after the 2D P,N,S-$Mo_2C$ test, while 2D $Mo_2C$ had a large decline. The corresponding CV curve is shown in Supplementary Figure 12. In addition, in the accelerated durability test, the scanning rate was 100 mV·s$^{-1}$, and 3,000 CV curves were recorded before and after scanning; the displacement of the polarization curve is negligible compared to the initial curve, consistently demonstrating excellent HER performance [Figure 5I].

Additionally, the electrocatalytic HER performance of Pt/C, 2D $Mo_2C$, 2D P-$Mo_2C$, 2D N-$Mo_2C$, 2D S-$Mo_2C$, 2D P,N-$Mo_2C$, 2D P,S-$Mo_2C$, 2D N,S-$Mo_2C$ and 2D P,N,S-$Mo_2C$ was also explored in 1 M KOH electrolyte. Figure 6A presents the polarization curves of the prepared samples and the Pt/C catalyst in an acidic medium. The sample achieves a current density of 10 mA·cm$^{-2}$ with only a 70 mV overpotential,

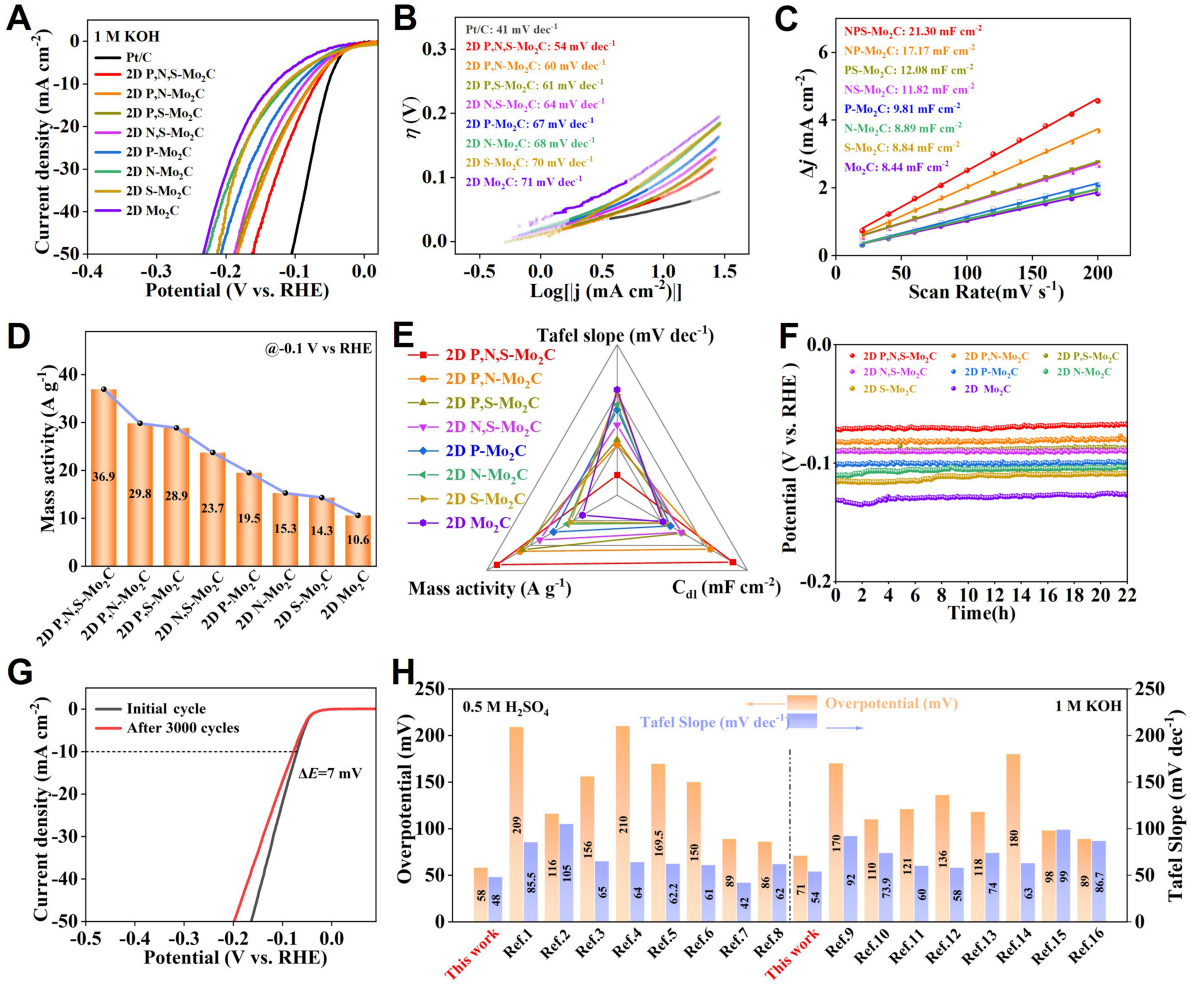


**Figure 6.** Synthesis of doped 2D $Mo_2C$ in 1 M KOH electrocatalytic HER by microwave pulse method. (A) Polarization curve; (B) The corresponding Tafel slope; (C) Plotting current density variation against scan rate to fit linear regression allows for the estimation of $C_{dl}$; (D) Mass activity of various spinels calculated at -0.1 V *vs.* RHE; (E) Summary of statistical electrochemical properties; (F) Chronopotentiometry test at the current density of 10 mA·cm$^{-2}$; (G) The accelerated durability tests of 2D P,N,S-$Mo_2C$; (H) The 2D P,N,S-$Mo_2C$ was compared with the overpotential and Tafel of other recently reported doped $Mo_2C$-based electrocatalysts. 2D: Two-dimensional; $Mo_2C$: molybdenum carbides; HER: hydrogen evolution reaction; RHE: reversible hydrogen electrode.

second only to Pt/C (52 mV). This value is 6~61 mV, lower than unary and binary doping $Mo_2C$ and pure $Mo_2C$ samples [Supplementary Figure 13]. In contrast, the performance of 2D P,N,S-$Mo_2C$ was improved greatly, consistent with the results measured in acidic media. The corresponding Tafel slopes of the polarization curves are shown in Figure 6B. The Tafel slope corresponding to the polarization curve is shown in Figure 6B. The Tafel slope of 2D P,N,S-$Mo_2C$ is 54 mV·dec$^{-1}$, again superior to 2D P-$Mo_2C$ (67 mV·dec$^{-1}$), 2D N-$Mo_2C$ (68 mV·dec$^{-1}$), 2D S-$Mo_2C$ (70 mV·dec$^{-1}$), 2D P,N-$Mo_2C$ (60 mV·dec$^{-1}$), 2D P,S-$Mo_2C$ (61 mV·dec$^{-1}$) , 2D N,S-$Mo_2C$ (64 mV·dec$^{-1}$) and much better than 2D $Mo_2C$ (71 mV·dec$^{-1}$). It shows that 2D P,N,S-$Mo_2C$ also has good reaction kinetics in an alkaline environment. In addition, CV curves of seven samples were measured in the potential range of 0.1 to 0.2 V (*vs.* RHE) [Supplementary Figure 14]. On this basis, the $C_{dl}$ of 2D P,N,S-$Mo_2C$ is estimated to be 21.30 mF·cm$^{-2}$, also the highest compared to other samples [Figure 6C]. The samples were similarly tested under alkaline conditions at -0.1 V *vs.* RHE for their MA values. Notably, the MA of 2D P,N,S-$Mo_2C$ at 36.9 A·g$^{-1}$ is 3.48 times higher than that of 2D $Mo_2C$ (10.6 A·g$^{-1}$) [Figure 6D]. As shown in Figure 6E, compared with other samples, 2D

P,N,S-$Mo_2C$ is the best in various tests, significantly exceeding 2D $Mo_2C$, consistent with the trend in acidic media. Under alkaline conditions, the long-term stability of eight samples was also evaluated using chronopotentiometry at a current density of 10 $mA·cm^{-2}$. The experimental results are consistent with those measured under acidic conditions. After 22 h of uninterrupted operation, the sample potential and electrochemical properties were almost unchanged [Figure 6F]. $C_{dl}$ was also tested after long-term cyclic stability, and the results showed that 2D P,N,S-$Mo_2C$ also had excellent stability in alkaline [Supplementary Figure 15]. The corresponding CV curve is shown in Supplementary Figure 16. Also, in the accelerated durability test, the polarization curve displacement is negligible compared with the initial curve, and the excellent HER performance is always maintained [Figure 6G]. As shown in Supplementary Figure 17A, XRD showed that 2D P,N,S-$Mo_2C$ exhibits no significant change before and after the screening; SEM images of 2D P,N,S-$Mo_2C$ after the durability test show that it still maintains a 2D form and no aggregation is observed [Supplementary Figure 17B]. In addition, HRTEM images of 2D P,N,S-$Mo_2C$ after stability testing show that the (100) face of 2D P,N,S-$Mo_2C$ has lattice fringes with a distinct spacing of 0.26 nm [Supplementary Figure 17C]. Finally, as shown in Figure 6H, we summarized the overpotentials and Tafel slopes of doped $Mo_2C$-based materials in acidic and alkaline electrolytes in recent years. It is noteworthy that 2D P,N,S-$Mo_2C$ shows the best HER performance, making it promising for practical applications. For more information, see Supplementary Tables 2 and 3.

## CONCLUSIONS

In summary, we propose a method for the one-step synthesis of highly tunable non-metal-doped 2D $Mo_2C$ using microwave pulses. This strategy utilizes the transient start-stop characteristics of microwave pulses to address the challenge of uncontrollable doping atom percentages in conventional approaches. Subsequently, the successful construction of 2D $Mo_2C$ doped with different typical non-metal elements at similar concentrations enabled a comprehensive elucidation of the specific impact mechanisms of non-metal doping on the electronic configuration-dependent electrocatalytic performance of 2D $Mo_2C$. Among them, phosphorus doping configurations may have the greatest positive impact, and the equiatomic 2D P,N,S-$Mo_2C$ exhibits outstanding HER performance, with a low overpotential of 58 mV at a current density of 10 $mA·cm^{-2}$ and a small Tafel value of 48 $mV·dec^{-1}$. We expect this strategy will enable the precise design of non-metallic atomic doping configurations in 2D TMCs and further explore the structure-activity mechanism in electrocatalytic applications, providing new insights for carbon neutrality and clean energy development.

## DECLARATIONS

### Acknowledgments

The authors acknowledge financial support from the National Natural Science Foundation of China (No. 52203070) and the Open Fund of Hubei Key Laboratory of Biomass Fiber and Ecological Dyeing and Finishing (No. STRZ202203). Wan J expresses gratitude for the financial support provided by the China Scholarship Council (CSC) Visiting Scholar Program.

### Authors' contributions

Contributed equally to this work and conceptualization: Fan M, Guo J, Fang G
Data curation and Writing - original draft: Fan M, Guo J
Formal analysis: Fan M, Fang G, Tian H, You Y
Software: Fang G, Huang Z, Huang J
Funding acquisition: Wan J, Xu W, Jiang H
Supervision, validation and writing - review and editing: Wan J

### Availability of data and materials
Not applicable.

### Financial support and sponsorship
This work was supported by the National Natural Science Foundation of China (No. 52203070) and the Open Fund of Hubei Key Laboratory of Biomass Fiber and Ecological Dyeing and Finishing (No. STRZ202203). Wan J expresses gratitude for the financial support provided by the China Scholarship Council (CSC) Visiting Scholar Program.

### Conflicts of interest
All authors declared that there are no conflicts of interest.

### Ethical approval and consent to participate
Not applicable.

### Consent for publication
Not applicable.

### Copyright
© The Author(s) 2024.

## REFERENCES
1. Yu H, Wan J, Goodsite M, Jin H. Advancing direct seawater electrocatalysis for green and affordable hydrogen. *One Earth* 2023;6:267-77. DOI
2. Liu W, Niu X, Tang J, et al. Energy-efficient anodic reactions for sustainable hydrogen production via water electrolysis. *Chem Synth* 2023;3:44. DOI
3. Wang J, Xu F, Jin H, Chen Y, Wang Y. Non-noble metal-based carbon composites in hydrogen evolution reaction: fundamentals to applications. *Adv Mater* 2017;29:1605838. DOI PubMed
4. Pang J, Sun J, Zheng M, Li H, Wang Y, Zhang T. Transition metal carbide catalysts for biomass conversion: a review. *Appl Catal B Environ* 2019;254:510-22. DOI
5. VahidMohammadi A, Rosen J, Gogotsi Y. The world of two-dimensional carbides and nitrides (MXenes). *Science* 2021;372:eabf1581. DOI PubMed
6. Jin H, Song T, Paik U, Qiao S. Metastable two-dimensional materials for electrocatalytic energy conversions. *Acc Mater Res* 2021;2:559-73. DOI
7. Peng X, Chen L, Liu Y, et al. Strain engineering of two-dimensional materials for energy storage and conversion applications. *Chem Synth* 2023;3:47. DOI
8. Jin H, Gu Q, Chen B, et al. Molten salt-directed catalytic synthesis of 2d layered transition-metal nitrides for efficient hydrogen evolution. *Chem* 2020;6:2382-94. DOI
9. Lu C, Tranca D, Zhang J, et al. Molybdenum carbide-embedded nitrogen-doped porous carbon nanosheets as electrocatalysts for water splitting in alkaline media. *ACS Nano* 2017;11:3933-42. DOI
10. Peng F, Zhang L, Jiang B, et al. In-situ synthesis of microflower composed of N-doped carbon films and $Mo_2C$ coupled with Ni or FeNi alloy for water splitting. *Chem Eng J* 2022;427:131712. DOI
11. Ma G, Ning G, Wei Q. S-doped carbon materials: synthesis, properties and applications. *Carbon* 2022;195:328-40. DOI
12. Ma X, Ning G, Wang Y, et al. S-doped mesoporous graphene microspheres: a high performance reservoir material for Li S batteries. *Electrochim Acta* 2018;269:83-92. DOI
13. Niu J, Dai P, Qi G, et al. Preparation of P doped $TiO_2$ nanotubes and its photocatalytic activity. *Integr Ferroelectr* 2016;176:150-9. DOI
14. Li C, Jang H, Liu S, et al. P and Mo dual doped Ru ultrasmall nanoclusters embedded in P-doped porous carbon toward efficient hydrogen evolution reaction. *Adv Energy Mater* 2022;12:2200029. DOI
15. Wan J, Zhang G, Jin H, et al. Microwave-assisted synthesis of well-defined nitrogen doping configuration with high centrality in carbon to identify the active sites for electrochemical hydrogen peroxide production. *Carbon* 2022;191:340-9. DOI
16. Lu F, Zhou Y, Liu J, Pan Y. Enhancement of F-doping on the electrochemical behavior of carbon-coated $LiFePO_4$ nanoparticles prepared by hydrothermal route. *Electrochim Acta* 2011;56:8833-8. DOI
17. Joucken F, Tison Y, Le Fèvre P, et al. Charge transfer and electronic doping in nitrogen-doped graphene. *Sci Rep* 2015;5:14564. DOI

PubMed PMC

18. Wang Y, Niu Y, Pu Y, Li S, Liu Y, Zhang B. Revealing the dynamic formation mechanism of porous $Mo_2C$: an *in-situ* TEM study. *Chem Synth* 2023;3:42. DOI
19. Jia Y, Zhang L, Zhuang L, et al. Identification of active sites for acidic oxygen reduction on carbon catalysts with and without nitrogen doping. *Nat Catal* 2019;2:688-95. DOI
20. de la Torre B, Švec M, Hapala P, et al. Non-covalent control of spin-state in metal-organic complex by positioning on N-doped graphene. *Nat Commun* 2018;9:2831. DOI PubMed PMC
21. Hasegawa G, Deguchi T, Kanamori K, et al. High-level doping of nitrogen, phosphorus, and sulfur into activated carbon monoliths and their electrochemical capacitances. *Chem Mater* 2015;27:4703-12. DOI
22. Liang HW, Zhuang X, Brüller S, Feng X, Müllen K. Hierarchically porous carbons with optimized nitrogen doping as highly active electrocatalysts for oxygen reduction. *Nat Commun* 2014;5:4973. DOI PubMed
23. Lv Q, Si W, He J, et al. Selectively nitrogen-doped carbon materials as superior metal-free catalysts for oxygen reduction. *Nat Commun* 2018;9:3376. DOI PubMed PMC
24. Zheng YR, Wu P, Gao MR, et al. Doping-induced structural phase transition in cobalt diselenide enables enhanced hydrogen evolution catalysis. *Nat Commun* 2018;9:2533. DOI PubMed PMC
25. Jin S, Guo Y, Wang J, Wang L, Hu Q, Zhou A. Carbon dioxide adsorption of two-dimensional $Mo_2C$ MXene. *Diam Relat Mater* 2022;128:109277. DOI
26. Tao Q, Dahlqvist M, Lu J, et al. Two-dimensional $Mo_{1.33}C$ MXene with divacancy ordering prepared from parent 3D laminate with in-plane chemical ordering. *Nat Commun* 2017;8:14949. DOI PubMed PMC
27. Khazaei M, Arai M, Sasaki T, Estili M, Sakka Y. The effect of the interlayer element on the exfoliation of layered $Mo_2AC$ (A = Al, Si, P, Ga, Ge, As or In) MAX phases into two-dimensional $Mo_2C$ nanosheets. *Sci Technol Adv Mater* 2014;15:014208. DOI PubMed PMC
28. Buke GC, Caylan OR, Ogurtani OT. Growth mechanism of 2D $Mo_2C$ on Cu via CVD. *Cryst Growth Des* 2023;23:5462-8. DOI
29. Geng D, Zhao X, Chen Z, et al. Direct synthesis of large-area 2D $Mo_2C$ on in situ grown graphene. *Adv Mater* 2017;29:1700072. DOI PubMed
30. Xu C, Wang L, Liu Z, et al. Large-area high-quality 2D ultrathin $Mo_2C$ superconducting crystals. *Nat Mater* 2015;14:1135-41. DOI PubMed
31. Xie H, Feng Y, He X, et al. Construction of nitrogen-doped biphasic transition-metal sulfide nanosheet electrode for energy-efficient hydrogen production via urea electrolysis. *Small* 2023;19:e2207425. DOI PubMed
32. Sun A, Shen Y, Wu Z, Wang D. N-doped MoP nanoparticles for improved hydrogen evolution. *Int J Hydrogen Energy* 2017;42:14566-71. DOI
33. Jiang H, Xian J, Hu R, et al. Microwave discharge for rapid introduction of bimetallic-synergistic configuration to conductive catecholate toward long-term supercapacitor. *Chem Eng J* 2023;455:140804. DOI
34. Jiang H, Li J, Xiao Z, et al. The rapid production of multiple transition metal carbides *via* microwave combustion under ambient conditions. *Nanoscale* 2020;12:16245-52. DOI
35. Wan J, Huang L, Wu J, et al. Microwave combustion for rapidly synthesizing pore-size-controllable porous graphene. *Adv Funct Mater* 2018;28:1800382. DOI
36. Xie H, Liu N, Zhang Q, et al. A stable atmospheric-pressure plasma for extreme-temperature synthesis. *Nature* 2023;623:964-71. DOI
37. Hu R, Jiang H, Xian J, et al. Microwave-pulse sugar-blowing assisted synthesis of 2D transition metal carbides for sustainable hydrogen evolution. *Appl Catal B Environ* 2022;317:121728. DOI
38. Xian J, Jiang H, Wu Z, et al. Microwave shock motivating the Sr substitution of 2D porous $GdFeO_3$ perovskite for highly active oxygen evolution. *J Energy Chem* 2024;88:232-41. DOI
39. Fang G, Liu K, Fan M, et al. Unveiling the electron configuration-dependent oxygen evolution activity of 2D porous Sr-substituted $LaFeO_3$ perovskite through microwave shock. *Carbon Neutralization* 2023;2:709-20. DOI
40. Hu R, Wei L, Xian J, et al. Microwave shock process for rapid synthesis of 2D porous $La_{0.2}Sr_{0.8}CoO_3$ perovskite as an efficient oxygen evolution reaction catalyst. *Acta Phys Chim Sin* 2023;39:2212025. DOI
41. Han K, Liu Z, Li P, et al. High-throughput fabrication of 3D N-doped graphenic framework coupled with $Fe_3C$@porous graphite carbon for ultrastable potassium ion storage. *Energy Storage Mater* 2019;22:185-93. DOI
42. Luo Y, Liu K, Jin H, Wang Z, Dai S, Huang L. Blowing ultrathin 2D materials. *Adv Mater Inter* 2023;10:2202239. DOI
43. Wang X, Zhang Y, Zhi C, et al. Three-dimensional strutted graphene grown by substrate-free sugar blowing for high-power-density supercapacitors. *Nat Commun* 2013;4:2905. DOI PubMed PMC
44. Zhou E, Wang C, Shao M, Deng X, Xu X. $MoO_2$ nanoparticles grown on carbon fibers as anode materials for lithium-ion batteries. *Ceram Int* 2017;43:760-5. DOI
45. Sun J, Chen X, Mao Z, Liu B, Zhao R, Du J. Fabrication of $Mo_2C$ nanoparticles on N-doped carbon nanosheets as high-performance electrocatalyst. *J Alloys Compd* 2023;934:167931. DOI
46. Wang D, Liu T, Wang J, Wu Z. N, P (S) Co-doped $Mo_2C$/C hybrid electrocatalysts for improved hydrogen generation. *Carbon* 2018;139:845-52. DOI
47. Yu B, Yang D, Hu Y, He J, Chen Y, He W. $Mo_2C$ nanodots anchored on N-doped porous CNT microspheres as electrode for efficient Li-ion storage. *Small Methods* 2019;3:1800287. DOI

48. Fan J, Wu X, Piñeiro-García A, et al. β-$Mo_2C$ nanoparticles produced by carburization of molybdenum oxides with carbon black under microwave irradiation for electrocatalytic hydrogen evolution reaction. *ACS Appl Nano Mater* 2021;4:12270-7. DOI
49. Zuo P, Liu Y, Liu X, Jiao W, Wang R. N, P-codoped molybdenum carbide nanoparticles loaded into N, P-codoped graphene for the enhanced electrocatalytic hydrogen evolution. *Int J Hydrogen Energy* 2022;47:29730-40. DOI
50. Geng W, Han H, Liu F, Liu X, Xiao L, Wu W. N,P,S-codoped C@nano-$Mo_2C$ as an efficient catalyst for high selective synthesis of methanol from $CO_2$ hydrogenation. *J CO2 Util* 2017;21:64-71. DOI
51. Wang Q, Yu R, Shen D, et al. One-pot synthesis of $Mo_2C$&$MoS_2$ loaded on N/S co-doped carbon materials as the electrocatalyts for hydrogen evolution reaction. *Fuel* 2022;318:123615. DOI
52. Wan J, Wu J, Gao X, et al. Structure confined porous $Mo_2C$ for efficient hydrogen evolution. *Adv Funct Mater* 2017;27:1703933. DOI
53. Zhao S, Lu X, Wang L, Gale J, Amal R. Carbon-based metal-free catalysts for electrocatalytic reduction of nitrogen for synthesis of ammonia at ambient conditions. *Adv Mater* 2019;31:1805367. DOI
54. Jiao Y, Zheng Y, Davey K, Qiao S. Activity origin and catalyst design principles for electrocatalytic hydrogen evolution on heteroatom-doped graphene. *Nat Energy* 2016;1:16130. DOI
55. Zhang Y, Yun S, Dang J, et al. Defect engineering via ternary nonmetal doping boosts the catalytic activity of ZIF-derived carbon-based metal-free catalysts for photovoltaics and water splitting. *Mater Today Phys* 2022;27:100785. DOI
56. Chang Y, Tseng C, Lee C, et al. N- and S-codoped graphene hollow nanoballs as an efficient Pt-free electrocatalyst for dye-sensitized solar cells. *J Power Sources* 2020;449:227470. DOI
57. Pei Z, Li H, Huang Y, et al. Texturing *in situ*: N,S-enriched hierarchically porous carbon as a highly active reversible oxygen electrocatalyst. *Energy Environ Sci* 2017;10:742-9. DOI
58. Wang X, Xia L, Guo C, et al. Interfacial engineering of N, S-doped $Mo_2C$-Mo/C heterogeneous nanorods for enhanced alkaline hydrogen evolution. *Appl Surf Sci* 2023;614:156276. DOI
59. Cai J, Song Y, Zang Y, et al. N-induced lattice contraction generally boosts the hydrogen evolution catalysis of P-rich metal phosphides. *Sci Adv* 2020;6:eaaw8113. DOI PubMed PMC
60. Xu J, Ge L, Zhou Y, et al. Insights into N, P, S multi-doped $Mo_2C$/C composites as highly efficient hydrogen evolution reaction catalysts. *Nanoscale Adv* 2020;2:3334-40. DOI PubMed PMC
61. Ji L, Wang J, Teng X, Dong H, He X, Chen Z. N,P-doped molybdenum carbide nanofibers for efficient hydrogen production. *ACS Appl Mater Interfaces* 2018;10:14632-40. DOI
62. Shi Z, Nie K, Shao Z, et al. Phosphorus-$Mo_2C$@carbon nanowires toward efficient electrochemical hydrogen evolution: composition, structural and electronic regulation. *Energy Environ Sci* 2017;10:1262-71. DOI
63. Zhu J, Mu S. Defect Engineering in carbon-based electrocatalysts: insight into intrinsic carbon defects. *Adv Funct Mater* 2020;30:2001097. DOI